Magnetically Modified Al_2O_3 Pillared Clays

A. P. Skoutelas, M. A. Karakassides, and D. Petridis*

Institute of Materials Science, NCSR "Demokritos", Ag. Paraskevi, Attikis, Athens 153 10, Greece

Received March 12, 1999. Revised Manuscript Received July 12, 1999

Surface modification of alumina pillared montmorillonite with magnetic iron oxide nanoparticles has been achieved by using as precursor a colloidal solution of magnetite in poly(vinyl alchohol). Two synthetic routes were developed differing in the number of steps. The magnetic and adsorption properties of the modified products were studied using Mössbauer spectroscopy, magnetization, and surface area measurements. All measurements showed that their magnetic and adsorption properties depend on the way of preparation. The Mössbauer spectra exhibited different superparamagnetic behavior for each modified product, whereas sorption analysis gave different surface areas and structural characteristics. TEM reveals the nano size of the iron oxides and furthermore their random dispersion at the external surfaces of the clay.

Introduction

Expandable layered aluminosilicate minerals are endowed with unique intercalation properties which render possible their transformation to restructured solids with promising advanced technological applications.[1−3] An important class of clay derivatives is pillared clays obtained from the insertion and grafting of metal oxidic species to the clay surfaces.[4−7] Possessing high surface area and microporosity, thermal stability, high Brønsted and Lewis surface acidity and molecular sieving properties, pillared clays act as efficient chemical catalysts in important organic reactions including oil cracking.

Advances in the field of pillared clays would be anticipated if the pillars were constructed from materials of high technological value, such as semiconductors, perovskites, magnetic oxides, or other important mixed-oxide catalysts.[8] Of equal importance would be solids derived from the encapsulation of such materials in the pores of a well-structured pillared clay, such as alumina, zirconia, or silica pillared clays. Finally, the uniform distribution of these materials on the surfaces of a delaminated pillared clay could also lead to fruitful innovations in material science. In all instances, immobilization of the metal oxide particles onto the host clay will restrict their agglomeration and therefore nanoscale magnetic clusters are expected to be formed.

Aiming at the development of such nanocomposites we describe here the use of stabilized colloidal dispersions of magnetite in poly(vinyl alcohol) (PVA)[9−11] as an effective system for the magnetic modification of clay surfaces. Since PVA is a potential complexant for the Keggin-like Al_{13} oligomeric cations, used in the synthesis of alumina pillared clay, we have made use of a PVA−magnetite hybrid as an appropriate system to induce magnetic modification of a parent alumina pillared clay. Magnetically modified pillared clays hold out the promise of providing new effective magnetic carriers suitable for a wide range of applications, including magnetic separation of biological systems[12−14] and magnetic supports for biotechnological applications.[15−17]

Experimental Section

Materials. The clay used in this study was a natural Wyoming montmorillonite, SWy-1. Prior to use, the clay was purified by sedimentation and converted to a homoionic Na^+-exchanged form by three ion exchange reactions with 1.0 M NaCl. The unit cell formula of the mineral is reported as $Na_{0.65}(Al_{3.04}Fe_{0.46}Mg_{0.50})(Si_{7.85}Al_{0.15})O_{20}(OH)_4$. The cationic exchange capacity is 80 mequiv/100 g. The polymer PVA with an averaged molecular weight of 22.000 was purchased from Aldrich. Iron sources were $FeCl_3 \cdot 6H_2O$ and $FeSO_4 \cdot 7H_2O$.

Synthesis of Colloidal Poly(vinyl alcohol) Magnetite. The PVA−magnetite composite was prepared by the method of Yokoi et al.,[9] which provides a good stoichiometry in magnetite. Specifically, 0.77 g of PVA were dissolved in 80 mL of hot distilled water and, after cooling, the required quantities of Fe^{3+} and Fe^{2+}, 0.21 g of $FeCl_3 \cdot 6H_2O$ and 0.12 g of $FeSO_4 \cdot$

* To whom correspondence should be addressed.

(1) Pinnavaia, T. J. *Science* **1983**, *220*, 365.
(2) Occelli, M. A.; Robson, H. *Expanded Clays and other Microporous Solids*; Academic Press: New York, 1992.
(3) Barrer, R. M. *Pure Appl. Chem.* **1989**, *61*, 1903.
(4) Mitchell, I. V. *Pillared Layered Structures. Current Trends and Applications*; Elsevier: London, 1990.
(5) Vaughan, D. E. W. *ACS Symp. Ser.* **1998**, *368*, 308.
(6) Burch, R. *Catal. Today* **1988**, *2*, 1−185.
(7) Ohtsuka, K. *Chem. Mater.* **1997**, *9*, 2039.
(8) Thomas, J. M. *Angew. Chem., Int. Ed. Engl.* **1988**, *27*, 1673.
(9) Yokoi, H.; Yagishita K.; Nakanishi, Y. *Bull. Chem. Jpn.* **1990**, *63*, 746.
(10) Fujiwara, S.; Fujiwara, Y. *J. Phys. Jpn.* **1962**, *17*, 405.
(11) Lee, J.; Isobe, T.; Senna, M. *J. Colloid Interface Sci.* **1996**, *177*, 490.
(12) Halling, P. J.; Dunnill, P. *Enzyme Microb. Technol.* **1980**, *2*, 2.
(13) Arshady, R. *Biomaterials* **1993**, *14*, 5.
(14) Kawaguschi, H. *Biomedical Applications of Polymeric Materials*; Tsuruta, T., Hayashi, T., Kataoka, K., Ishihara, K., Kimura, Y., Eds.; CRC Press: London, 1993.
(15) Robinson, P. J.; Dunnill, P.; Lilly, M. D. *Biotechnol. Bioeng.* **1973**, *14*, 597.
(16) Penchev, I. P.; Hristov, J. Y. *Powder Technol.* **1990**, *61*, 103.
(17) Rosensweig, R. E.; Siegel, J. H.; Lee, W. K.; Mikus, T. *AICHE Symp. Ser.* **1981**, *77*, 205.

10.1021/cm990150c CCC: $18.00
Published on Web 09/11/1999

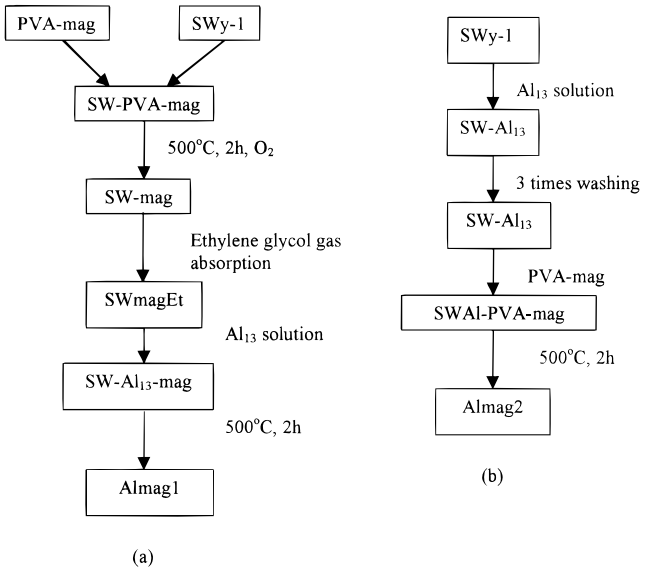

Figure 1. Synthetic pathways for the magnetic modification of the alumina pillared clay Almag1 (a) and Almag2 (b).

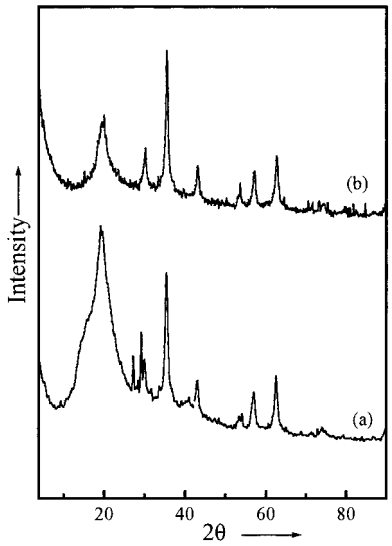

Figure 2. XRD patterns for PVA−magnetite (a) and PVA−magnetite after calcination at 500 °C (b).

$7H_2O$, were added with vigorous stirring. After complete dissolution, the pH of the solution was raised to 10.5 using 2 M NaOH. The solution was stirred under sealed state conditions for 1 day for further stabilization of magnetite. This colloidal solution, after centrifuging 3 times, was used as the modifier for the alumina pillared clay.

Synthesis of Magnetically Modified Alumina Pillared Clay. Two different procedures were followed to prepare magnetically modified solids, as illustrated in Figure 1. According to the first pathway, Figure 1a, a magnetite dispersion in PVA was reacted with sodium montmorillonite to give a product designated as SW−PVA−mag. This was isolated by centrifugation, washed with water and air-dried by spreading on a glass plate. This material was then heated to 500 °C for 2 h under an O_2 atmosphere. The XRD pattern of the calcined solid showed a collapsed clay structure (d_{001} = 10.23 Å). To swell the collapsed structure the material was treated with ethylene glycol in a gas absorption process to facilitate the solvent function (SWmagEt). A sample of SWmagEt was dissolved in water and then reacted with a solution containing the $[Al_{13}O_4(OH)_{24}(H_2O)_{12}]^{7+}$ oligomer,[18,19] followed by centrifugation, washing, and air-drying to give SW−Al_{13}−mag. Thermal treatment of SW−Al_{13}−mag at 500 °C for 2 h (O_2 atmosphere) gave the final product which will from now on be referred as **Almag1**.

In the second route, a solution containing the $[Al_{13}O_4(OH)_{24}(H_2O)_{12}]^{7+}$ oligomer was reacted with an aqueous suspension of clay according to well-established procedures. The resulting intermediate complex (SW−Al_{13}) was centrifuged, washed three times with water and then treated with a colloidal dispersion of PVA−magnetite. The new product was isolated by centrifugation, washed with water, and air-dried to give SWAl−PVA−mag. Finally, calcination of the last product at 500 °C at a slow rate of 0.2 °C/min to avoid the formation of carbon residue gave the final product, **Almag2**.

Characterization. Powder X-ray diffraction (PXRD) was performed with a Siemens D-500 powder diffractometer, using Cu Kα radiation. Magnetic measurements were carried out with a Quantum Design magnetometer. Mössbauer spectra were recorded with a constant acceleration Mössbauer spectrometer with a ^{57}Co (Rh) source. The parameters were obtained by a least-squares fit programm of the data on a PC with Lorentzian line shapes. Relative errors were less than ±0.01 mm s^{-1}. The system was calibrated with an iron foil absorber. Surface area measurements were carried out with a nitrogen porosimeter, Autosorb 1, Quantacrome Corporation. The samples were outgassed at 53 K for 48−72 h under high vacuum (10^{-5} mbar) in the outgassing section of the apparatus. A CM 20 Phillips instrument was used for the transmission electron microscopy pictures. Finally, the inductively coupled argon plasma (ICP) spectrometric method was used for the chemical analysis of the final products.

Results and Discussion

Characterization of PVA−Magnetite Composite. This nonclay composite was characterized by XRD and Mössbauer measurements. The diffraction pattern, Figure 2a, shows characteristic peaks of an iron spinel structure which can be attributed to either magnetite (Fe_3O_4) or to the structurally isomorphous maghemite (γ-Fe_2O_3). The amorphous background and the broad shoulder at the left side of the reflection peak around 20° is attributed to PVA. Owing to this background, identification of the less pronounced lines, which could help to differentiate magnetite from maghemite, is difficult.[20,21] Calcination of the PVA−magnetite at 500 °C gave a similar XRD pattern but without the broad shoulder (Figure 2b). To distinguish more accurately the nature of iron species and evaluate better the magnetic properties of the composite, we resort to Mössbauer spectroscopy.

Figure 3 shows the Mössbauer spectra for a PVA−magnetite composite at room, liquid nitrogen, and liquid helium temperatures. The spectra are not characteristic of stoichiometric bulk magnetite.[22,23] However, it is known that fine particles of magnetite immobilized on carriers such as polymers or surfactants,[24−26] give spectra that possess Mössbauer parameters different

(18) Johansson, G. *Acta Chem. Scand.* **1960**, *14*, 771.
(19) Bottero, J. Y.; Cases, J. M.; Fiessinger, F.; Poirier, J. E. *J. Phys. Chem.* **1980**, *84*, 2933.
(20) Daniels, J. M. D.; Rosencwaig, A. *J. Phys. Chem. Solids* **1969**, *30*, 1561.
(21) Da Costa, G. M.; De Grave, E.; De Bakker, P. M. A.; Vandenberghe, R. E. *Clays Clay Miner.* **1995**, *43*, 656.
(22) Roggwiller, P.; Kündig, W. *Solid State Commun.* **1973**, *12*, 901.
(23) McNab, T. K.; Fox, R. A.; Boyle, A. J. F. *J Appl. Phys.* **1968**, *39*, 5703.
(24) Kaiser, R.; Rosenweig, R. E. *Report CR-1407*; NASA: Washington, DC, 1969; p 1.
(25) Moskowitz, R. *IEEE Spectrum* **1975**, *12*, 53.
(26) Khalafalla, S. E. *CHEMTECH* **1975**, 540.

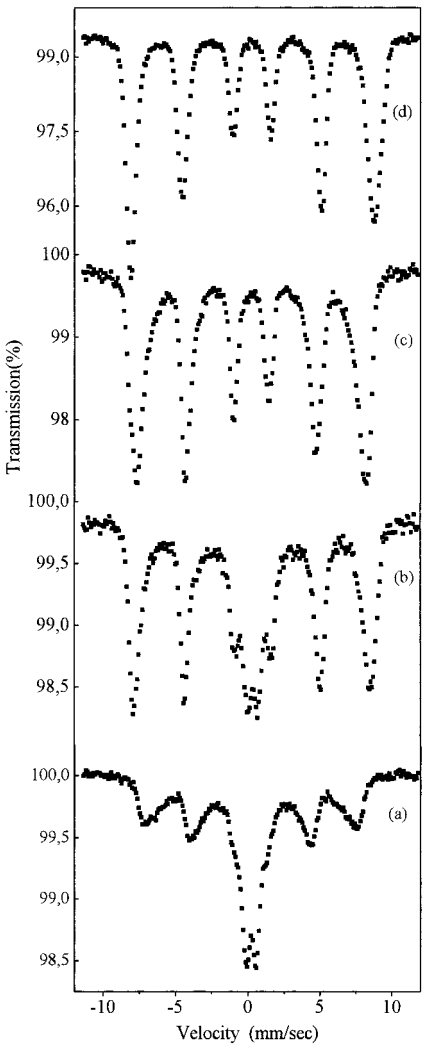

Figure 3. Mössbauer spectra for PVA−magnetite at room temperature (a), liquid nitrogen (b), and liquid helium (c) and after calcination at 500 °C and recorded at liquid nitrogen (d).

from those of bulk stoichiometric magnetite.[27] The spectrum at room temperature consists of a broad magnetic sextet with a superimposed quadrapole doublet. As the temperature is lowered to 80 and 4.2 K, the magnetically split lines become sharper and gain intensity at the expense of the quadrapole doublet. The magnetic to nonmagnetic ratio for the PVA−magnetite hybrid was found to vary from 2.59 at room temperature to 4.63 at 80 K, while the spectrum at 4.2 K was fully magnetically resolved. This temperature dependence of the spectra is characteristic of a superparamagnetic system consisting of small magnetic particles (∼100 Å) with a distribution of sizes.[28]

In general terms, in superparamagnetism, all spins of iron atoms within a particle point in the same direction, but thermal fluctuations cause this direction to vary with a frequency depending upon the particle size, anisotropy energy, and temperature. If this frequency is greater than the Larmor precession frequency of the ^{57}Fe nucleus (10^8 s^{-1}), the magnetic hyperfine splitting collapses to give a single line or a doublet if a quadrapole interaction is present. In the opposite case of slow relaxation of the iron spins, a complete magnetic hyperfine splitting is observed. However, because of particle size distribution in a sample the spectra typically consist of a doublet, due to small particles with a short relaxation time and a sextet due to larger particles with longer relaxation times.[28,29] Furthermore, the relative area of the doublet is expected to increase with increasing temperature as a result of the increasing relaxation frequency, and the magnetic sextet(s) to increase with lowering temperature as the relaxation frequency slows. According to this description, the superparamagnetic patterns exhibited by the PVA−magnetite composites reveal that the system consists of nanoscale magnetic particles with a distribution of sizes dispersed in the PVA matrix.

The Mössbauer spectrum recorded at room temperature in Figure 3 can be analyzed with a superparamagnetic doublet, two magnetic sextets with low IS values (0.36 and 0.47 mm s^{-1}) indicative of trivalent iron and a relaxation component displaying a high IS value (0.82 mm s^{-1}). This last component is attributed to a fast electron-hopping process taking part between divalent and trivalent iron species in the magnetite structure. The high IS value, which lies between typical trivalent and divalent iron values, advocates for the presence of magnetite in the colloidal precursor.

After calcination at 500 °C, the sample gave the liquid nitrogen Mössbauer spectrum shown in Figure 3d. It is now clear that the relaxation component is missing from the spectra. The spectrum could be analyzed with two magnetic sextets with low IS values (0.44 and 0.41 mm/s), which indicate the existence of only trivalent iron. Calcination, therefore, induced the oxidation of Fe^{2+} to Fe^{3+} and the subsequent transformation of magnetite to γ-Fe_2O_3 according to the well-known oxidation reaction of magnetite to maghemite under oxidative conditions:[30]

$$4Fe_3O_4 + O_2 \rightarrow 6Fe_2O_3 \qquad (1)$$

In addition, both magnetic components have zero quadrapole splitting values, a result which excludes the formation of α-Fe_2O_3 during calcination of the PVA−magnetite hybrid. Given that γ-Fe_2O_3 undergoes a structural transition to α-Fe_2O_3 at temperatures higher than 350 °C,[31] the Mössbauer results demonstrate the stabilizing effect of PVA on γ-Fe_2O_3. Finally, the absence of superparamagnetic doublet in the calcined spectra clearly reveals that particle sintering during heat treatment increased the iron oxide size and transformed the small oxidic species to bulk γ-Fe_2O_3.

Characterization of Magnetically Modified Alumina Pillared Clay. The diffraction patterns in Figure 4 refer to products in the first synthetic pathway for producing material Almag1. The XRD pattern for SWmag in diagram 4a indicates an almost collapsed

(27) Hassett, R. L.; Stecher L. C.; Hendrickson, D. N. *Inorg. Chem.* **1980**, *19*, 416.
(28) Mørup, S.; Dumesic, J. A.; Topsøe, H. *Applications of Mössbauer Spectroscopy*; Cohen, R. L., Ed.; Academic Press: New York, 1980; Vol. II.
(29) Vandenberghe, R. E.; De Grave, E. *Mössbauer Spectroscopy Applied to Inorganic Chemistry*; Long, G. J., Grandjean, F., Eds.; Plenum Press, New York, 1989; Vol. 3.
(30) Chang, H. S. W.; Chiou, C. C.; Chen Y−W. *J. Solid State Chem.* **1997**, *128*, 87.
(31) Nikumbh, A. K.; Latkar, A. A.; Phadke, M. M. *Thermochim. Acta* **1993**, *219*, 269.

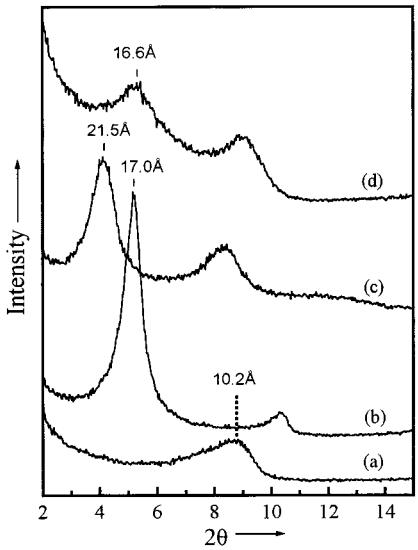

Figure 4. XRD patterns according to the first synthetic pathway for Almag1 material.

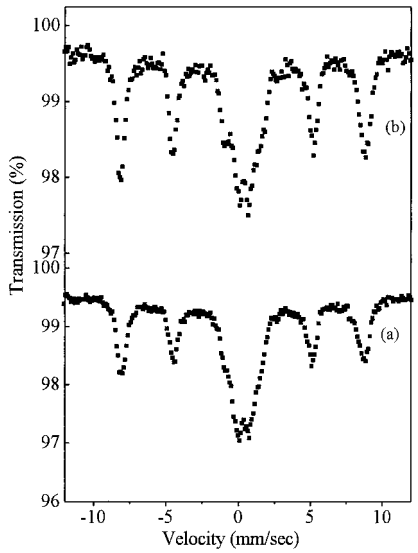

Figure 5. Mössbauer spectra for Almag1 at liquid nitrogen (a) and liquid helium (b).

structure (10.2 Å). The difference between the value of the totally collapsed structure (theoretical value ~9.6 Å) and the observed can be attributed either to a layer of very fine oxidic particles or to the presence of carbon residue. The peak at 17.0 Å in diagram 4b indicates the ability of ethylene glycol to effectively swell the SWmag solid. The peak shift to 21.5 Å in diagram 4c ($SWAl_{13}$-mag) clearly shows the intercalation of the Al_{13} pillaring agent. Finally, Figure 4d for the magnetic product Almag1 gives a basal space of 16.6 Å, corresponding to an interlayer gallery of about 7 Å.

Mössbauer spectra for sample Almag1, recorded at 77 and 4.2 K, are shown in Figure 5. The spectra demonstrate clearly superparamagnetic behavior as the ratio of magnetic to superparamagnetic area changes from 1.09 at 77 K to 1.57 at 4.2 K. The superparamagnetic behavior implies that the magnetic oxides keep their nanoscale size by being finely dispersed on the surfaces and galleries of the alumina pillared structure despite the thermal treatment at 500 °C. Apparently, the clay sheets strongly pin the fine particles, preventing their

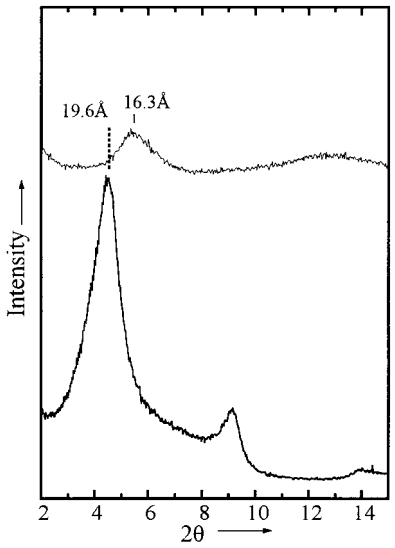

Figure 6. XRD patterns according to the second synthetic pathway for Almag2 material.

agglomeration in the course of calcination. The spectra were analyzed with one superparamagnetic doublet and two magnetic sextets with relatively low isomer shift values (0.47 and 0.51 mm/s) which is indicative of trivalent iron. This result is expected, since calcination at 500 °C to form a pillared clay, transforms magnetite to γ-Fe_2O_3, as we have already seen in the calcination of PVA−magnetite composite.

The diffraction patterns from products obtained according to the second synthetic route are shown in Figure 6 (bottom air dried and top calcined at 500 °C). The diffraction line centered at 19.59 Å, which is attributed to the intercalated alumina species and also to the colloidal PVA−magnetite precursor. The calcination step reduced the d_{001} basal spacing to 16.26 Å, which corresponds to an interlayer distance of about 6.7 Å. A final verification of the iron spinel oxides on the clay surfaces in both methods of preparation arises from a detailed examination of the X-ray patterns of the final products in the region 30−70°. The diffraction lines observed in this region, clearly show the presence of the same iron oxidic species at the external surfaces of the two final alumina pillared clays. Furthermore the Mössbauer spectra of product Almag2 recorded at 77 and 4.2 K are shown in Figure 7. Superparamagnetic features are again present with a magnetic to superparamagnetic portion increasing from 0.58 at 77 K to 0.94 at 4.2 K.The analysis of the spectra shows two magnetic components with isomer shift values characteristic of trivalent iron. These results lead again to the conclusion that the magnetic phase is γ-Fe_2O_3, is finely dispersed on the pillared clay surfaces with a size distribution giving rise to a superparamagnetic doublet superimposed on a magnetic sextet. Furthermore, the Mössbauer analysis shows that while the increase in the ratio of magnetic to superparamagnetic area with decreasing the temperature from 77 to 4.2 K is about 62% for Almag2, the analogous increase for Almag1 sample is about 44%. Almag2 therefore has a greater superparamagnetic portion in comparison with Almag1. This probably results from the different thermal treatments used during the synthetic pathways. The Almag2 solid was treated once at 500 °C in a final step, while

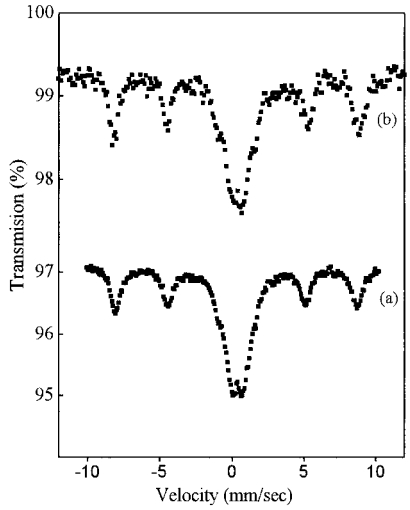

Figure 7. Mössbauer spectra for Almag2 at liquid nitrogen (a) and liquid helium (b).

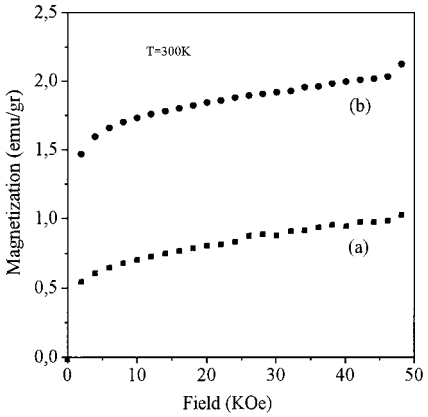

Figure 8. Magnetization versus applied magnetic field at room temperature for Almag2 (a) and Almag1 (b).

Table 1. Magnetization at Room Temperature and Iron Oxide Content for the Final Materials

	Fe_2O_3 (wt %)	M_s (emu/g of product)	M_s (emu/g of Fe_2O_3)
Almag1	5.77	2.03	35
Almag2	4.53	1.04	23

Almag1 was treated at this temperature twice. Thus, even if clay matrix can prevent particle agglomeration, repeated thermal treatments seems to induce an increment in the volume of particles, which in turn, enhances the magnetic portion of the spectrum.

Magnetization measurements show also that Almag1 has a higher loading in magnetic γ-Fe_2O_3 than Almag2. Figure 8 shows the variation of magnetization versus applied magnetic field at room temperature for the two final products. The saturation magnetization for Almag1 is almost 2 emu/g while for Almag2 is about 1 emu/g. From the chemical analysis results, we have estimated the magnetization of the final products according to their theoretical content in γ-Fe_2O_3 (Table 1). The enhanced loading of γ-Fe_2O_3 in Almag1 is attributed to the different synthetic routes. Indeed, as Almag1 was treated with the colloidal precursor in an initiative step, before exchange with Al_{13} ions, the clay surfaces were able to adsorb a greater amount of the PVA−magnetite precursor. In the second route, the clay was first treated with an Al_{13} solution whereupon its surfaces were partially occupied by hydroxoaluminum species. The ensuing loading restricts the insertion of the PVA−magnetite colloid in the clay galleries and gives a lower magnetic component in comparison with the first route.

Table 2. Surface Area Data for the Final Products as Received from BET Method and *t*-Plots[a]

	Almag1	Almag2
S_{BET} ($m^2\,g^{-1}$)	116	205
S_t ($m^2\,g^{-1}$)	139	223
S_{micro} ($m^2\,g^{-1}$)	34.88	140
S_{meso} ($m^2\,g^{-1}$)	81.42	64.9
V_{MP} (mL)	0.0240	0.0546
d_{MP} (Å)	6	6

[a] Where S_{BET} is the BET surface area, S_t is the total surface area, S_{micro} and S_{meso} are the micropore and mesopore surface area respectively, V_{MP} is the micropore volume, and d_{MP} is the average micropore diameter.

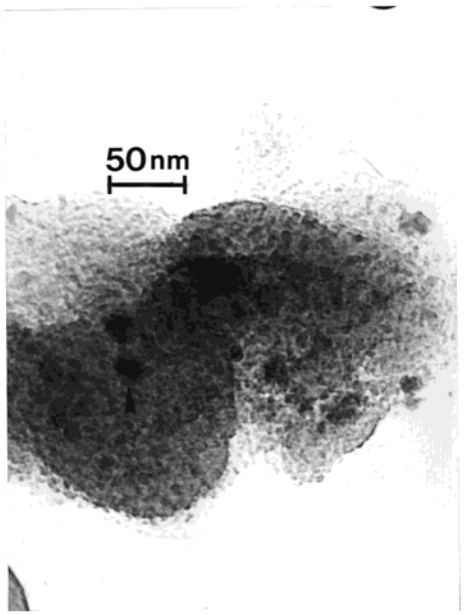

Figure 9. Transmission electron micrograph of Almag2.

The pore structures of the Almag1 and Almag2 solids were also examined by N_2 absorption−desorption measurements. The absorption data were treated by the BET equation in the range of linearity and by the *t*-plot method.[32] The BET surface area for Almag2 (205 m^2g^{-1}), (see Table 2), is almost twice that of Almag1 (116 m^2g^{-1}), a result ascribed to the combined effect of different degree of iron oxide loading and thermal treatment. The chemical analysis shows that Almag1 has a higher γ-Fe_2O_3 loading. The nano γ-Fe_2O_3 particles located near clay edges obscure the insertion of nitrogen molecules into the galleries, and therefore, a lower surface area results. On the other hand, it is known that high-temperature treatment causes a partial collapse in a pillared structure and therefore reduces its porosity. Accordingly, Almag1, which was treated two times at 500 °C, has another reason to exhibit lower porosity.

The adsorption data were also analyzed by *t*-plots. These plots were typical for microporous materials in the presence of mesopores. From Table 2 we can see that the mesoporous structure contributes almost equally to

(32) De Boer, J. H.; Lippens, B. C.; Linsen, B. G.; Broekhoff, J. C. P.; Van den Heuvel, A.; Osinga, Th. J. *J. Colloid Interface Sci.* **1966**, *21*, 405.

the surface of the final pillared clays while the microporous proportion is clearly higher in Almag2. These results suggest that mesopores, which are probably created from voids in sheet arrangements, are independent of iron oxide loading. The average diameter estimated from *t*-plots (6 Å) is consistent with the interlayer distance from the XRD results.

Finally, a TEM photograph of Almag2 material is shown in Figure 9. From this picture we can see that particles of γ-Fe_2O_3 have been scattered randomly on the external surfaces of the alumina pillared clay. We do not observe regions with γ-Fe_2O_3 aggregates, while particle size fluctuates between 5 and 25 nm. The small size of these particles confirms again that the clay surfaces act as an immobilization substrate for the nanosized oxides.

Conclusions

The main conclusions of the present work are as follows:

(1) Smectite clays can be modified with magnetite using as precursor a stabilized aqueous colloid of PVA−magnetite as a precursor.

(2) Calcination at 500 °C of the clay−PVA−Fe_3O_4 nanocomposite does not lead to a magnetic oxide pillared clay but to a collapsed structure with magnetic oxide particles uniformly dispersed on the clay surfaces.

(3) Alumina pillared smectites modified with uniformly dispersed γ-Fe_2O_3 particles on their surfaces have been prepared by two different routes.

(4) The alumina pillared clay−γ-Fe_2O_3 nanocomposites exhibit superparamagnetic behavior which manifests the ability of the clay substrate to immobilize the fine iron particles and to prevent their aggregation to larger particles.

(5) Supplementary techniques complete the image of the structure and properties of the magnetically modified alumina pillared clays. Porosimetry shows that the final surface area depends on the number of calcination steps and the extent of loading of the alumina pillared clay with iron oxides. Finally, it was estimated from TEM that the size of γ-Fe_2O_3 particles fluctuates between 5 and 25 nm.

Acknowledgment. Helpful discussions with Dr. A. Simopoulos are gratefully acknowledgment. This work was partially supported by Greek Secretariat of Research and Technology through the YPER program and by the Silver & Baryte Ores Mining Co, Athens, Greece.

CM990150C